Printing Small Dots from Large Drops

Emma L. Talbot[†], *Huai N. Yow*[‡†], *Lisong Yang*[†], *Arganthaël Berson*[‖], *Simon R. Biggs*[‡†] *and Colin D. Bain*[†]*

[†]Department of Chemistry, Durham University, Stockton Rd, Durham, DH1 3LE, U. K. [‡]Institute of Particle Science and Engineering (IPSE), School of Process, Environmental and Materials Engineering, University of Leeds, Leeds LS2 9JT, U. K. [‖]School of Engineering and Computing Sciences, Durham University, Stockton Rd, Durham, DH1 3LE, U. K.

Keywords: Droplet deposition, inkjet printing, drying, depletion flocculation, sol-gel transition

Printing of droplets of pure solvents containing suspended solids typically leads to a ring stain due to convective transport of the particles towards the contact line during evaporation of the solvent. In mixtures of volatile solvents, recirculating cells are established that lead to migration of colloidal particles towards the centre of the droplet. In favourable cases, a dense disk of particles forms with a diameter much smaller than that of the droplet. In the latter stages of drying, convective transport of the particles radially towards the contact line still occurs. Two strategies are described to fix the distribution of particles in a compact disk much smaller than the diameter of the drying droplet. First, a nano-particulate clay is added to induce an evaporation-driven sol-gel transition that inhibits convective flow during the latter stages of drying. Second, a non-adsorbing polymer is added to induce depletion flocculation that restricts

particle motion after the particles have been concentrated near the centre of the droplet. The area of the resulting deposit can be as little as 10% of the footprint of the printed droplet.

Introduction

Ring stains are the common result of the evaporation of droplets containing dissolved solutes or suspended solids. The coffee ring left by spilt coffee is one familiar example. A ring stain arises in pinned droplets from the enhanced evaporation of the solvent near the edge of the droplet. To maintain the spherical cap shape of the droplet, capillary flow replenishes solvent lost due to evaporation, transporting particles to the contact line [1]. In inkjet printing applications, the resulting dot has lower optical density at the centre compared to the edge leading to poor image quality and the need for an excess of ink to generate a desired depth of colour. Non-uniform deposits are also detrimental to inkjet printing applications such as organic electronics [2–5], printed circuit-boards [6–9], and biomedicine (e.g. micro-assays) [10,11]. Internal flows driven by surface-tension gradients – known as Marangoni flows – have been used to counteract the formation of a ring stain and produce more uniform deposits [12–16], enhancing print quality or performance.

Marangoni flows can be induced by thermal gradients, by surfactants or by differential evaporation in solvent mixtures (a well-known example being the tears of wine in a glass) [12,17,18].

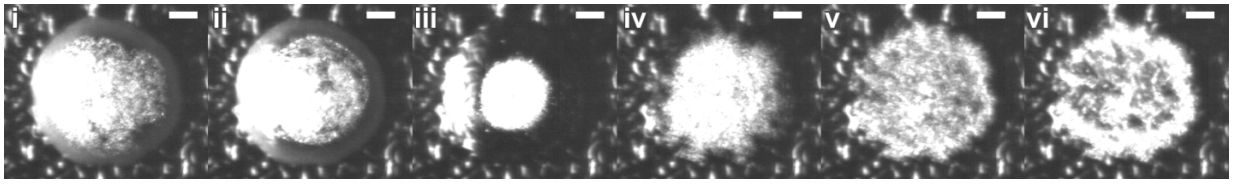

Figure 1. Dark field images of a drying 50%v ethanol/water droplet containing 0.1%v 1 μm polystyrene spheres after i) $0.1t_{dry}$, ii) $0.2t_{dry}$, iii) $0.5t_{dry}$, iv) $0.8t_{dry}$, v) $0.9t_{dry}$ and vi) $1.0t_{dry}$ (where $t_{dry} = 2.80$ s). Scale bars are 20 μm. A ring stain deposit is formed.

The evaporation-driven Marangoni flows in ethanol/water mixtures not only re-circulate particles within the droplet but also lead to migration of particles across the streamlines towards the centre of the droplet [19,20] (see Figure 1). Particle migration creates a concentrated central group of particles and a region near the contact line that is depleted of particles. At some stage during the evaporation, the Marangoni recirculation abruptly ceases (Figure 1(iii)) and is replaced by evaporation-driven radial flow that transports particles towards the contact line leading to dissipation of the collected group (Figure 1(iv)-(v)). The final result is a ring stain (Fig. 1(vi)) [20].

The driving force for the cross-stream migration is still not entirely clear and various possible mechanisms will be considered elsewhere. Here, we concern ourselves with the practical question of how we can 'fix' the particle distribution in a concentrated central disk before radial flow transports particles to the periphery. The ability to print a dot with a diameter much smaller than the initial droplet footprint could be useful for security printing. Extending the concept to lines of coalesced droplets would allow the printing of wires or tracks much finer than the droplets used to print the lines. In this paper, we describe and compare two strategies. The first strategy involves addition of a nanoparticulate clay. As the droplet evaporates, the concentration of the clay increases to the point where it undergoes a sol-gel transition. The resulting elasticity in the droplet dominates the capillary forces and inhibits the formation of a ring stain [21]. We have shown previously that the sol-gel transition in pure water droplets can be used to generate a deposit with a uniform profile. The challenge here is to time gelation to coincide with the

minimum in the diameter of the collected group of particles. The second strategy involves the addition of a non-adsorbing polymer that is excluded from the region between colloidal particles and induces an attractive, osmotic force between them. As the droplet evaporates, the polymer concentration and hence the attractive force increases leading to aggregation of the particles, a process known as depletion flocculation. The challenge is to induce flocculation of the collected particles into a single, connected aggregate without premature aggregation that leads to a lumpy deposit. The physical chemistry of these two strategies is described in greater detail below.

Sol-gel transition

Laponite (a nano-particulate clay) forms shear-thinning suspensions that can be jetted from an inkjet print-head. The high shear in the print-head breaks down the networked structure of the laponite suspension. As the droplet dries, the laponite is concentrated and the network recovers, undergoing a sol-gel transition [21]. The increased yield stress and elastic modulus of the gel [22] can resist the capillary stresses that otherwise result in radial particle motion. We define a dimensionless number

$$\varepsilon = G' r_c / 2\sigma \qquad [1]$$

as the ratio of the elastic modulus, G', to the Laplace pressure ($p = 2\sigma/r_c$) inside the droplet, where r_c is the radius of curvature of the droplet and σ is the surface tension. In order to resist deformation, ε must be at 1. For a 50%v ethanol/water suspension with surface tension, σ = 29 mN m^{-1}, droplet height, h = 7 μm, contact radius, R = 80 μm, and contact angle, θ = 10°, the Laplace pressure, p = 126 Pa (where the radius of curvature, $r_c = (R^2+h^2)/2h$). Note that p depends on the radius of curvature. If droplet dries with a constant contact angle (receding contact line), p increases during drying. In the presence of suspended solids, it is much more common for the contact line to be pinned and then p decreases during drying.

For droplets with a contact angle below 90°, evaporation is fastest at near the contact line [1]. The droplet is also thinner near the contact line and hence the laponite concentration increases fastest near the periphery of the droplet: it is here that the suspension gels first. A gelling front propagates from the contact line inwards, preventing particle motion in the gel. Figure 2 illustrates this process for polystyrene spheres in a pure water droplet (in pure water there is no cross-stream migration and so there are particles throughout the droplet to enable us to visualise the flow). Varying the initial laponite concentration enables us to induce gelation at the time when the particles are most densely packed near the droplet centre and thus to prevent radial flow outward at the end of drying.

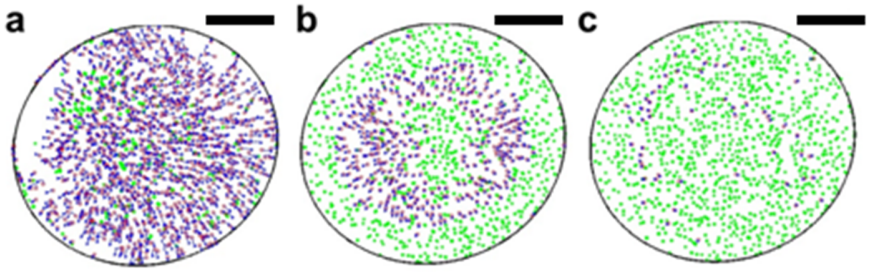

Figure 2. Particle tracks within a drying droplet of 2%w laponite in pure water between a) 0.0-0.1t_{dry}, b) 0.4-0.5t_{dry}, and c) 0.7-0.8t_{dry} (where t_{dry} = 6.32 s). Stationary particles are in green, moving particles are in blue with their initial position marked in red. The contact line is marked by a black ellipse. Scale bars are 50 μm.

The alternative fixing strategy explored in this paper uses a non-adsorbing polymer (polystyrene sulfonate) to induce depletion flocculation of the particles once they have migrated to the centre of the droplet. Depletion flocculation [23–25] can occur when particles approach each other to less than the twice the radius of gyration of the particle. It is energetically more favourable for the polymer to leave the gap between the particles than to change its conformation

in order to fit within the restricted volume between approaching particles. As a consequence, the water solvent between the particles has a lower polymer concentration than the bulk solution and there is an osmotic pressure forcing the particles together. The strength of the depletion force and the compactness of the aggregates depend on the concentration and molecular weight of the polymer and on the particle concentration [26]. Lower molecular-weight polymers lead to a shallower minimum in the free energy since the particles need to be closer together before the polymers are excluded from the contact (and hence the osmotic pressure acts over a shorter range). The weaker depletion interaction allows reversible detachment and rearrangement of particles, resulting in a denser and more compact floc structure. However, a higher polymer concentration is required to induce flocculation at lower polymer molecular weights. Since aggregation involves the loss of translational entropy of particles, higher polymer concentrations are also required to aggregate particles at lower particle concentrations. During evaporation, both the polymer concentration and the particle density increase, favouring flocculation.

Experimental Methods

Inkjet droplets were formed with a Microfab device (MJ-ABP-01, Horizon Instruments, 50 μm) controlled by a Microfab JetDrive III Controller. The particle distribution inside a drying droplet was imaged on an inverted microscope using dark-field illumination. Images were acquired at 250 frames per second with an exposure of 100 μs (Photron APX RS) from below through the substrate. Transparent glass substrates were plasma-coated with a hydrophobic layer as described in [27] to increase contact angles. The drying time, t_{dry}, was defined as the time when the refractive index contrast of the beads changed due to loss of solvent over the top of the beads.

Sol-gel mechanism. Laponite suspensions (RD grade, Rockwood, disks 30 nm across and 1 nm thick, according to the manufacturer's specifications) were prepared in ethanol/water mixtures. The laponite was first added gradually, with agitation, to high-purity water (MilliQ) or to a suspension of polystyrene spheres (1 μm diameter, 0.1%v concentration, University of Leeds) and sonicated until the laponite formed a clear suspension. Ethanol (Sigma Aldrich, 99.9%) was then added and sonicated until clear. The order of addition was important, as adding the laponite to an ethanol/water mixture resulted in a cloudy flocculated suspension even after sonication. The laponite does not alter the surface tension [28] enough to prevent solutal Marangoni flows.

Depletion flocculation. Polystyrene sulfonate (PSS) was used as the non-adsorbing polymer with the following molecular weights: 35 kg mol^{-1} (Scientific Polymer Products Inc.), 70 kg mol^{-1} (Sigma Aldrich), 300 kg mol^{-1} (Alfa Aesar), and 500 kg mol^{-1} (Alfar Aesar). The PSS was dissolved in high-purity water and left overnight. Ethanol was then added and the solution was shaken to ensure homogeneous mixing. Last, 755 nm polystyrene spheres (University of Leeds, in ethanol) were added to give a concentration of 0.1%v.

Rheological data for laponite suspensions were collected at 293 K in an AR 2000 Rheometer (TA Instruments) with a cone (2° angle) and plate geometry, without the inclusion of polystyrene spheres. The steady-state viscosity of each fluid was recorded over shear rates from 0.001-1500 s^{-1}. Recovery times were investigated by applying a stepped shear rate with fast sampling. The shear rate was held at 0.1 s^{-1} for 10 minutes, then 1000 s^{-1} for 4 minutes, before returning to the low shear value (0.1 s^{-1}). The yield stress of each laponite suspension was found using oscillatory measurements with small deformations, performed with a strain sweep (for strain values between the rheometer's lower limit of 2.88×10^{-3} and 0.35) at a frequency of 1 Hz. The yield stress was estimated from the product of the critical strain and the elastic modulus in the linear elastic

region. The critical strain was defined as the strain at which a straight-line fit to the linear elastic region and non-linear viscoelastic region intersected.

A LUMiSizer® 611 (L.U.M. GmbH) was used for the centrifugal sedimentation of polystyrene particles in suspension (as in [29]). Suspensions containing 5%v polystyrene spheres (630 nm, University of Leeds) were observed at varying PSS content. Samples of 400 μL were placed in a polycarbonate cell (optical path length 2.0 mm) and spun at 1500 rpm for 10 hours to form an initial packed sediment bed. The centrifugation field was then increased step-wise by 500 rpm every 84 minutes up to a maximum of 4000 rpm. Stable particles (no aggregates) form a flat, packed bed. Aggregates are able to withstand the applied centrifugal force, forming a less compressed sediment bed, and thus giving a raised bed height (see Figure 3). Increasing the centrifugation field can further compact the bed with weaker aggregates collapsing at lower spinning rates.

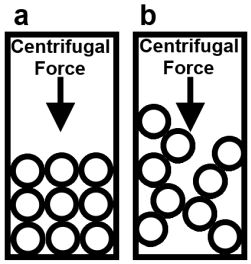

Figure 3. Schematic illustration of the sediment bed from a) stable particles, b) aggregated particles. The sediment bed is more compressed with a lower bed height for stable particles.

Dried deposits were imaged with a scanning electron microscope (SEM, Philips XL30 Environmental SEM) to determine the packing and distribution of the polystyrene spheres. The deposits were sputter coated with gold (three coats at 1.2 kV, 35 mA for 30 s, Edwards Scancoat Six) before imaging.

Results and Discussion

In ethanol/water mixtures, circulating flows developed during drying, coupled with particle migration. Figure 4 shows the progress of the evaporation of droplets of ethanol/water mixtures of varying compositions, imaged through the substrate. The radius of the particle group, R_g (see Figure 5), decreased throughout the Marangoni flow period, reaching a minimum radius, $R_{g,min}$, at a time, t_{Rg}, that coincided with the point when Marangoni flow ceased. Subsequently, capillary flow transported particles towards the contact line, increasing R_g again (see Figure 1, not shown in Fig. 4).

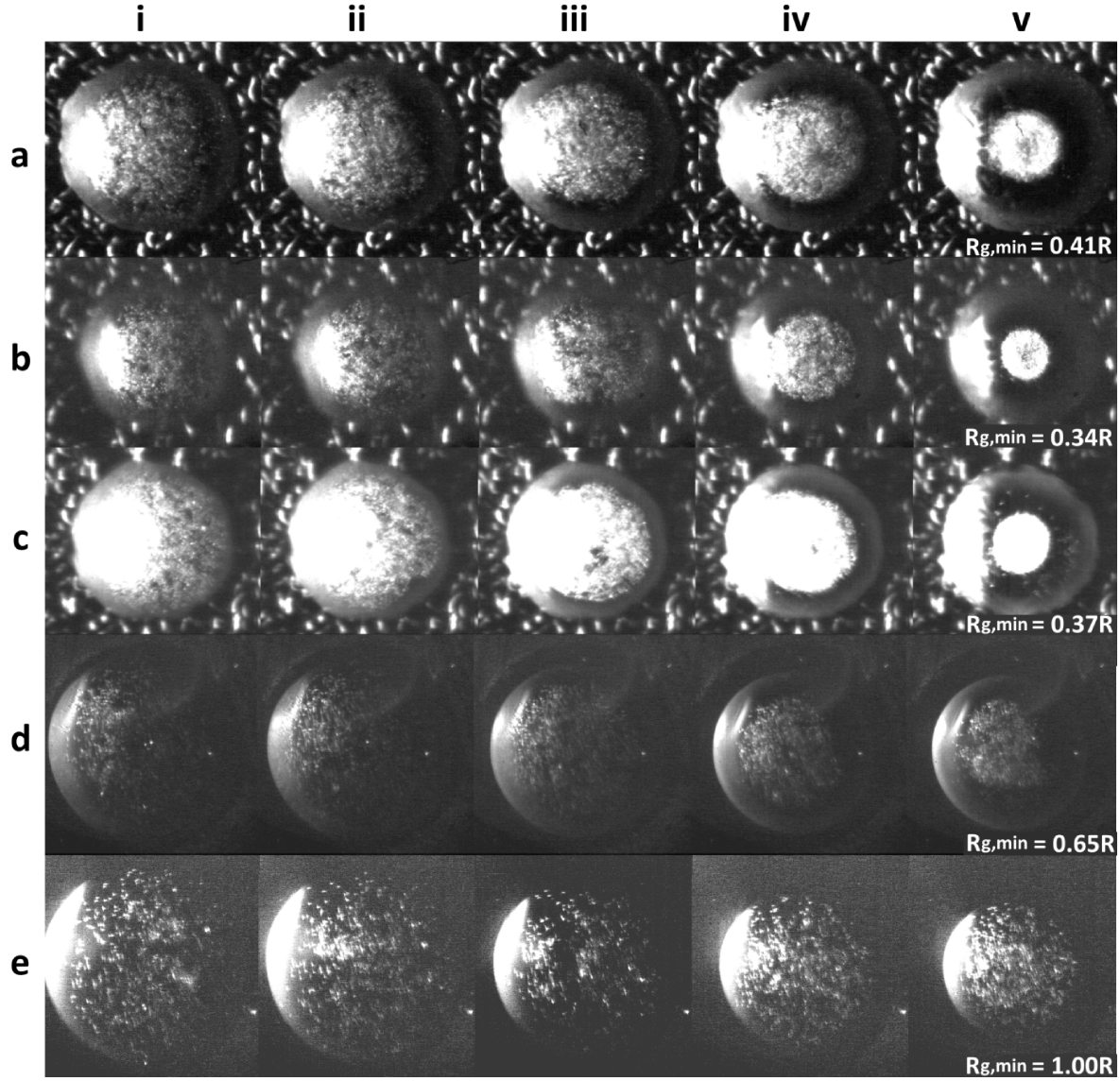

Figure 4. Drying droplets containing a) 10%v, b) 30%v, c) 50%v, d) 70%v, or e) 90%v ethanol/water and 0.1%v 1 μm polystyrene spheres on coated substrates after i) $0.1t_{Rg}$, ii) $0.2t_{Rg}$, iii) $0.5t_{Rg}$, iv) $0.8t_{Rg}$ and v) $1.0t_{Rg}$. The minimum radius of the group, $R_{g,min}$, is shown as a fraction of the contact radius at time t_{Rg}.

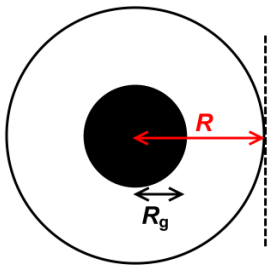

Figure 5. Schematic of the particle group (with radius R_g) in a droplet of contact radius R.

Particle migration was most pronounced in lower ethanol concentrations (10-50%v) with $R_{g,min}$ reaching a minimum value of 0.34 for 30%v ethanol. At 70%v ethanol, the collected group was twice as wide and for 90%v ethanol no particle migration was evident. Therefore, water-rich mixtures produce the most concentrated particle groups.

Sol-gel fixing strategy

Control of the rheology of laponite/ethanol/water suspension is essential to fix the distribution of polystyrene particles at the minimum radius, R_g. If the suspension gels too late, the particles will be transported outwards by capillary flow. If the viscoelasticity increases too soon, the Marangoni flows and particle migration will be suppressed. At the same time, the high-shear rheology must be compatible with inkjet printing. Figure 4 shows that particle migration is most pronounced in mixtures that are initially ≤ 50%v ethanol. During evaporation, the concentration of ethanol drops further so at the point of gelation the %v of ethanol is less than that in the original formulation. We therefore need to explore only the rheology of water-rich suspensions. We take 10%v and 50%v ethanol as the limits of the relevant formulation space (the rheology of laponite in pure water has been described in [27]).

Inverted bottle experiments for laponite/ethanol/water mixtures place the sol-gel transition between 2.8-3.0%w laponite in 10%v ethanol/water (the same as in pure water [21]) and between

1.5-2.0%w laponite in 50%v ethanol/water. Hence, the gel point is lowered at higher ethanol concentrations. This trend hinders the fixing strategy: as ethanol is depleted during drying the laponite concentration required to reach the gel point increases progressively.

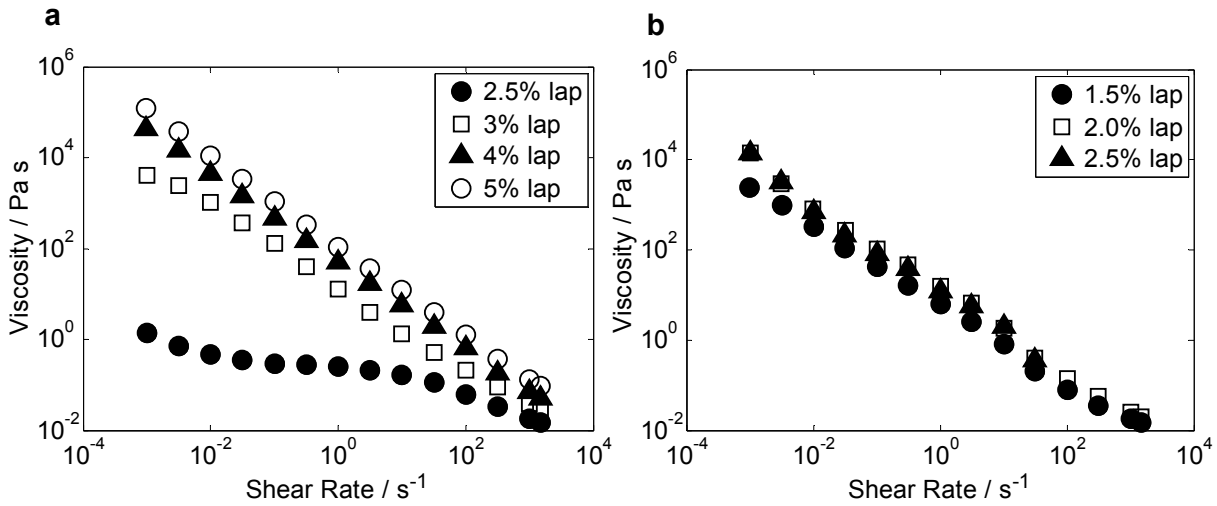

Figure 6. Shear viscosity of laponite suspensions in a) 10%v ethanol/water and b) 50%v ethanol, with various laponite concentrations over a range of shear rates.

The shear-thinning properties of the laponite suspensions are displayed in Figure 6. The network structure responsible for the high viscosity at low shear breaks down under the shear rates in the nozzle of the print-head (~10^4 s^{-1} for the Microfab) to give a low viscosity fluid (viscosity, $\eta \sim 10^{-2}$ Pa s). In the 10 %v ethanol suspension, the viscosity increased with increasing laponite concentration. For the same laponite concentration (2.5 %w) the mixture with more ethanol had a higher low-shear viscosity but a similar high-shear viscosity. Thus the jettability is unaffected by either the ethanol or laponite concentration within the range studied.

Table 1 displays the yield stress of the laponite suspensions shown in Figure 6. At the higher ethanol concentration, a yield stress is first observed at a lower laponite concentration (1.5 %w laponite in 50 %v ethanol compared to 3 %w laponite in 10 %v ethanol). The yield stress

increased markedly with laponite concentration at 10 %v ethanol but less so at 50 %v ethanol. The typical Laplace pressure in a drying droplet is ~ 100 Pa so the yield stress must be at least of this order for gelation to inhibit radial capillary flows. The data in Table 1 suggest that the gel in 50 %v ethanol may be too weak, but the gel becomes stronger as the ethanol evaporates.

Table 1. Yield stresses for laponite suspensions in ethanol/water mixtures.

Laponite / %w	Ethanol / %v	Yield Stress / Pa
2.5	10	-
3.0	10	6
4.0	10	29
5.0	10	99
1.5	50	5
2.0	50	26
2.5	50	24

It is not only the yield stress that is important for the success of our strategy but also the speed with which the laponite network recovers after a period of high shear: the minimum group radius is attained after a time t_{Rg} ~ 1 s for 50 pL drops. The laponite network thus needs to gel on a timescale of less than 1 s. Figure 7 presents the recovery of the shear viscosity of laponite suspensions following a period of high shear (and then a return to a low shear rate). Although we did not measure the elasticity directly, we assume that the elasticity recovers at the same speed as the viscosity. For fixed ethanol concentration, the shear viscosity recovered faster with higher laponite content. Similarly, a higher concentration of ethanol increased the speed at which the laponite network reformed for the same laponite concentration.

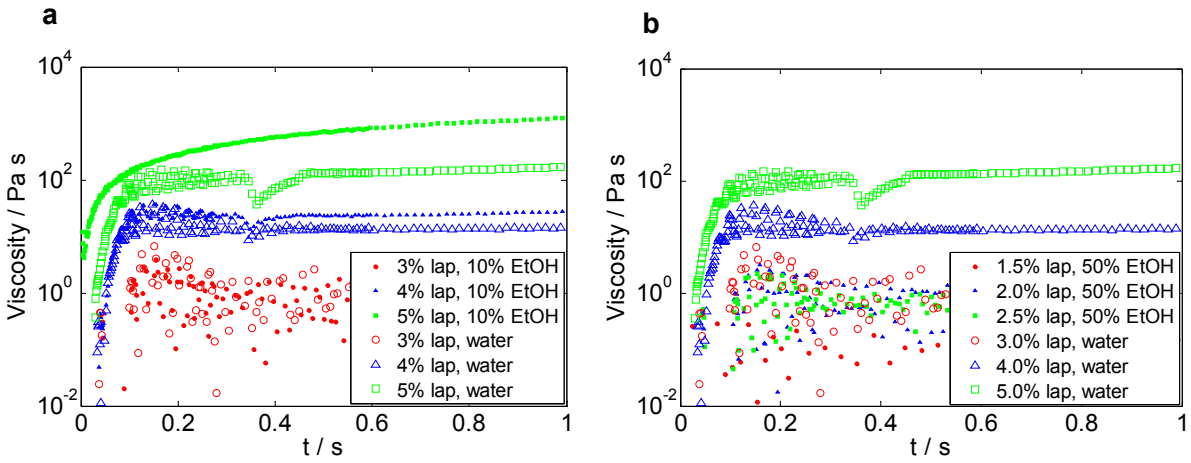

Figure 7. Recovery of the shear viscosity for laponite suspensions in a) 10%v ethanol and b) 50%v ethanol, compared to laponite/water suspensions with a laponite concentration following evaporation of the ethanol. Arrows show the change in composition during drying. The dip just before 0.4 s is an artefact due to the rheometer's response time.

As a droplet of laponite/ethanol/water dries, ethanol evaporates preferentially. Therefore, during drying, the ethanol concentration decreases and the laponite concentration increases, changing the composition towards a laponite suspension in pure water. An increase in the laponite concentration leads to faster recovery, but a decrease in ethanol content leads to an increase in the recovery time. The combined effect is a decreased recovery time. Figure 7 shows that the laponite network can recover within the drying lifetime for both water and ethanol/water mixtures.

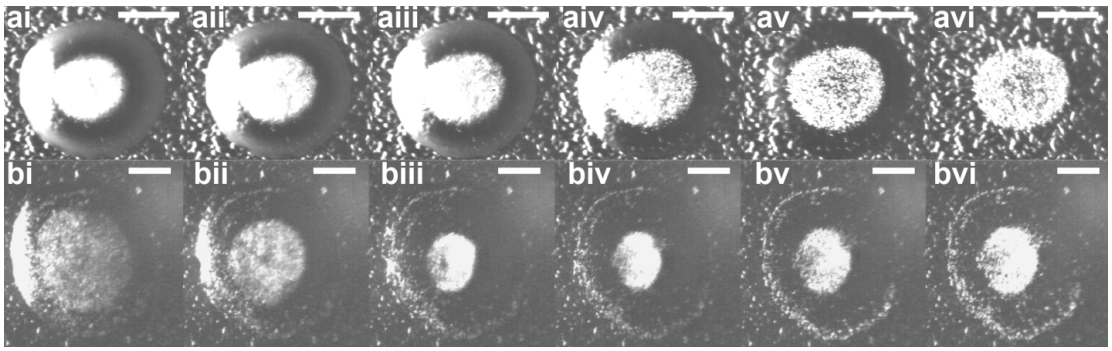

Figure 8. Images of drying droplets of laponite/ethanol/water suspensions containing 0.1%v 1 μm polystyrene spheres and a) 10%v ethanol with 2.5%w laponite, and b) 50%v ethanol with 1.5%w laponite. Images were taken after i) 0.1 t_{dry}, ii) 0.2 t_{dry}, iii) 0.3 t_{dry}, iv) 0.5 t_{dry}, v) 0.8 t_{dry} and vi) 1.0 t_{dry}. Scale bars are 50 μm.

We recorded the drying behaviour of 10%v and 50%v ethanol/water mixtures with varying concentrations of laponite. For 10%v ethanol, laponite concentrations below 2%w did not gel sufficiently quickly: the particles migrated inwards to form a central disk with a size similar to that in the absence of laponite, but were then transported towards the contact line by radial convection in the latter part of drying. For concentrations of laponite ≥2.0%w, the droplet gelled from the contact line inwards and halted the radial convection of the particles, fixing the centrally collected group. The minimum value of R_g in the dry deposit was obtained with 2.5%w laponite (Figure 8a). There was some outward motion of the collected group before the sol-gel transition supressed convection, giving a deposit diameter of $0.6R$ (where R is the initial radius of the contact line), compared to a value of $R_{g,min} = 0.41R$ observed in the absence of laponite (Figure 4a). At an initial laponite concentration ≥2.8%w, the viscosity near the contact line rose too quickly and prevented migration of particles near the contact line towards the central disk. The final deposit comprised a central dot and ring near the contact line.

Increasing the ethanol concentration to 50%v ethanol gave similar results to the 10%v ethanol, but at lower concentrations of laponite. Figure 8b shows the smallest central dot in the dry deposit, which was obtained with 1.5%w laponite, but also showing the peripheral ring.

The experiments described above show that the strategy of using the sol-gel transition in laponite suspensions to fix the central disk of particles does work, but that the minimum radius of the dry deposit is significantly larger than the minimum radius of the collected group in the

absence of laponite. Further increases in laponite concentration led to a peripheral ring in addition to a central dot. The best results were obtained for a 10%v ethanol/water mixture containing 2.5%w laponite. For this mixture the polystyrene sphere concentration was increased up to 1%v (no higher was tested), and still resulted in particle migration (though to a wider group radius) and small dot deposit (Figure 9).

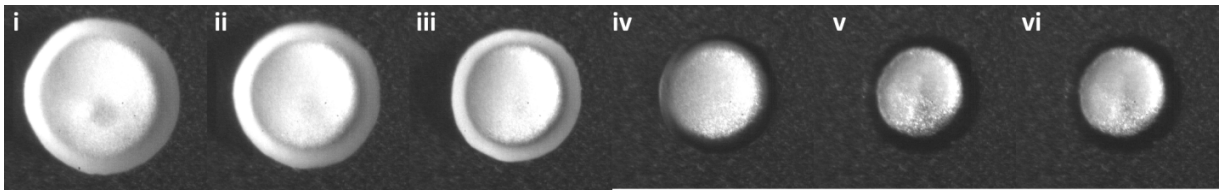

Figure 9. Sequence of images for a drying ethanol/water mixture containing 10%v ethanol, 2.5%w laponite and 1%v 775 nm polystyrene spheres at i) $0.1t_{dry}$, ii) $0.2t_{dry}$, iii) $0.5t_{dry}$, iv) $0.8t_{dry}$, v) $0.9t_{dry}$, vi) $1.0t_{dry}$.

Depletion flocculation

The second control strategy was based on depletion flocculation. A free polymer (polystyrene sulfonate, PSS) was included in the ethanol/water mixture. Sedimentation studies were carried out to determine the PSS concentration required to induce aggregation of the polystyrene spheres in water for PSS molecular weights of 70 kg mol^{-1}, 300 kg mol^{-1} and 500 kg mol^{-1}. The stability against aggregation in ethanol/water was assessed to ensure that most of the ethanol would need to evaporate before there was significant aggregation of the polystyrene spheres in order to inhibit aggregation while the particles were migrating towards the centre of the droplet.

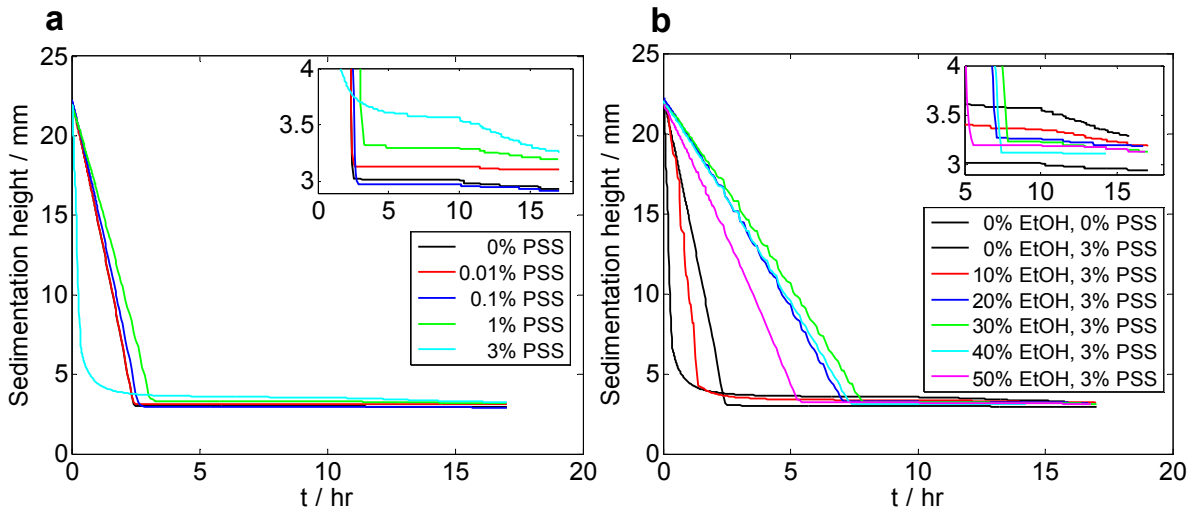

Figure 10. Sedimentation profiles of 5%v polystyrene spheres in a) water with increasing PSS (70 kg mol^{-1}) concentration and b) water with 0%w PSS (70 kg mol^{-1}) or ethanol/water solutions with 3%w PSS (in the water alone). Insets show zoom-ins for the beds following initial compression. The centrifuge speed was held at 1500 rpm for 10 hours then increased stepwise by 500 rpm every 84 minutes until a maximum of 4000 rpm.

Figure 10a shows the sedimentation profiles for 70 kg mol^{-1} PSS solutions in water at increasing PSS concentrations. At concentrations up to 0.1%w PSS, the similarity in the sedimentation profile to that of 0%w PSS indicates minimal particle aggregation. At a PSS concentration of 1%w, there are competing effects between the increase in viscosity due to the presence of the free polymer and the increase in floc size due to particle aggregation. Sediment bed compression indicates the presence of aggregated particles (leading to a more open bed); compared to stable particles with no added PSS. At 3%w PSS, there is clear evidence of particle aggregation in the steeper initial sedimentation profile and stepwise bed compression profile (following the increase of the centrifuge speed after 10 hours).

To formulate a PSS suspension in ethanol/water that will be stable in the print-head, but induce particle flocculation as the suspension becomes water-rich during drying, the sedimentation

profiles of particles within PSS (70 kg mol^{-1}) suspensions in a range of ethanol/water mixtures were investigated (see Figure 10b). Each suspension contained 3%w PSS in the water phase alone before dilution with ethanol to ensure flocculation on depletion of the ethanol. From here on, PSS concentrations are given in the water alone unless stated otherwise (e.g. 3%w PSS corresponds to a 1.7%w PSS concentration in the entirety of a 50%v ethanol/water). Figure 10b shows that ethanol/water suspensions containing 3%w PSS are stable if the ethanol concentration is ≥20%v. At lower concentrations of ethanol, the sediment bed was raised compared to that of 0%w PSS, and the steeper initial sediment profile indicates particle aggregation. Hence, an initial ethanol concentration of at least 20%v is required to ensure particle stability in the print-head.

Table 2. PSS concentration required to induce particle aggregation for three molecular weights (MW) of the polymer, and the minimum ethanol content for a stable suspension.

MW /kg mol^{-1}	PSS for aggregation in water/ %w	Min ethanol / %v
70	3.0	20
300	0.5	30
500	0.1	20

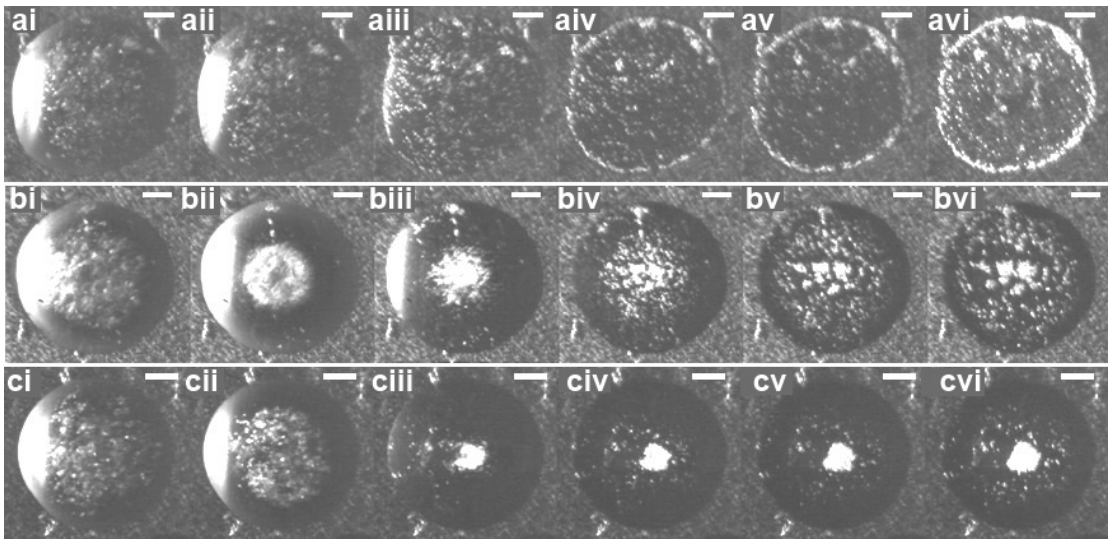

Figure 11. Drying droplets of 50%v ethanol containing 0.1%v 755 nm polystyrene spheres and a) 0.1%w, b) 1%w, c) 3%w PSS (70 kg mol^{-1}) after i) 0.1t_{dry}, ii) 0.2t_{dry}, iii) 0.5t_{dry}, iv) 0.8t_{dry}, v) 0.9t_{dry} and vi) 1.0t_{dry}. Scale bars are 20 μm. PSS concentrations are given in the water alone.

Lower PSS concentrations were required to induce particle flocculation at higher molecular weights (Table 2). For each molecular weight of PSS, at least 20-30%v ethanol was required for the suspension of PS particles to be stable. We chose to print particle suspensions in a 50%v ethanol/water mixture to ensure that the formulation was stable and did not flocculate during the migration period.

Figure 11 shows the effect on the deposit of adding 70 kg mol^{-1} PSS to a PS particle suspension in 50%v ethanol/water. At PSS concentrations ≤0.1%w (i.e. ≤0.06%w total in the entire suspension), drying progressed similarly to droplets without PSS. Particles collected during the Marangoni flow period and were subsequently transported to the contact line during the radial flow period to form a ring stain (Figure 11a(vi)). At 1%w PSS (i.e. 0.6%w in the entire suspension), some flocculation occurred in the collected group of particles, but the flocs were carried outwards by convective flow in the latter stages of drying. The result was a deposit consisting of large particle flocs at the centre and smaller particle flocs towards the contact line (Figure 11b(vi)). At a PSS concentration of 3%w (i.e. 1.7%w in the entire suspension), particle flocs "locked" together at the centre of the droplet to form one large floc from which only a few single particles escaped via radial flow (Figure 11c(vi)). This large floc settled onto the substrate under gravity and remained at the centre of the droplet, giving a deposit diameter of ~0.3R.

Figure 11 explores the effect of molecular weight on droplet drying. For higher molecular weights of PSS (300 kg mol^{-1} and 500 kg mol^{-1}), lower concentrations of PSS are required to induce flocculation – which is desirable – but the viscosity also increases more quickly with

molecular weight (Figure 13). If the viscosity increases too much during the early stages of drying, the Marangoni flows and the consequent particle migration are weaker due to the free polymer, which plays a key role in the structure of the end deposit (see Figure 12 (b),(c)). Figure 14 shows how the radius of the migrating group of particles varies with time for a range of concentrations of 300 kg mol^{-1} PSS. At PSS concentrations ≤0.5%w, the inward migration of particles was unhindered and the minimum radius of the collected group was the same as in the absence of PSS (~0.3*R*). When the PSS concentration increased to ≥1%w, the viscosity increase reduced migration, causing a wider collected group (~0.5*R*). As depletion flocculation is enhanced at higher particle concentrations [26], the wider particle group makes depletion flocculation less efficient. We observed the formation of small aggregates, which were transported towards the contact line by convection during the latter stages of drying with both 300 kg mol^{-1} and 500 kg mol^{-1} PSS (Fig 11). While the polymer concentration was high enough for flocculation (Table 2), the particle concentration was too low to form a single connected floc.

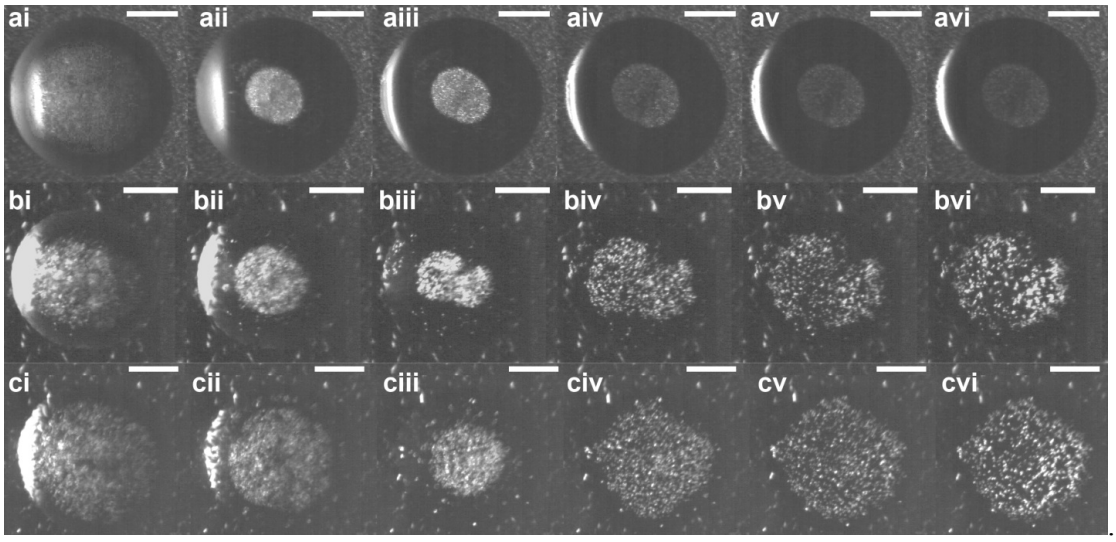

Figure 12. Drying droplets of 50%v ethanol containing 0.1%v 755 nm polystyrene spheres and a) 15%w PSS (35 kg mol^{-1}), b) 0.3%w PSS (300 kg mol^{-1}), and c) 0.3%w PSS (500 kg mol^{-1}) after

i) 0.1t_{dry}, ii) 0.2t_{dry}, iii) 0.5t_{dry}, iv) 0.8t_{dry}, v) 0.9t_{dry} and vi) 1.0t_{dry}. Scale bars are 50 μm. PSS concentrations are given in the water alone.

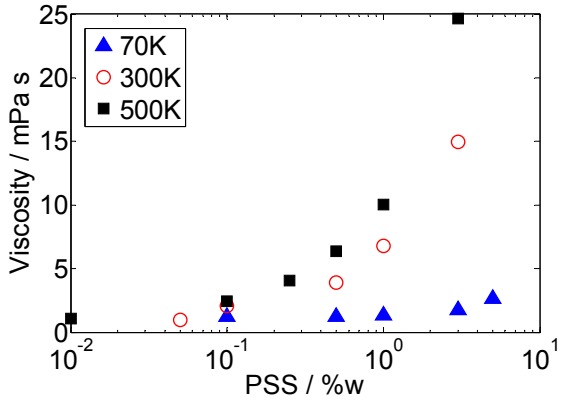

Figure 13. The dependence of the low-shear viscosity on the polymer concentration for various molecular weights of PSS.

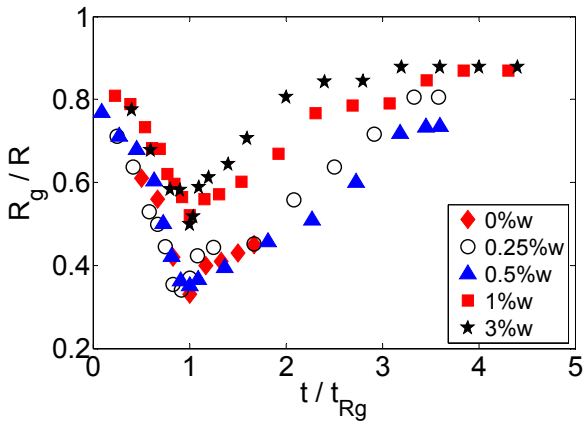

Figure 14. Evolution of the particle group radius, R_g, with time for a 50%v ethanol droplet containing 0.1%v 755 nm spheres and various concentrations of PSS (300 kg mol^{-1}) in the water alone. R_g is normalized by the initial droplet contact radius, R, and the time is normalized by the time at which the group reaches a minimum radius, t_{Rg}.

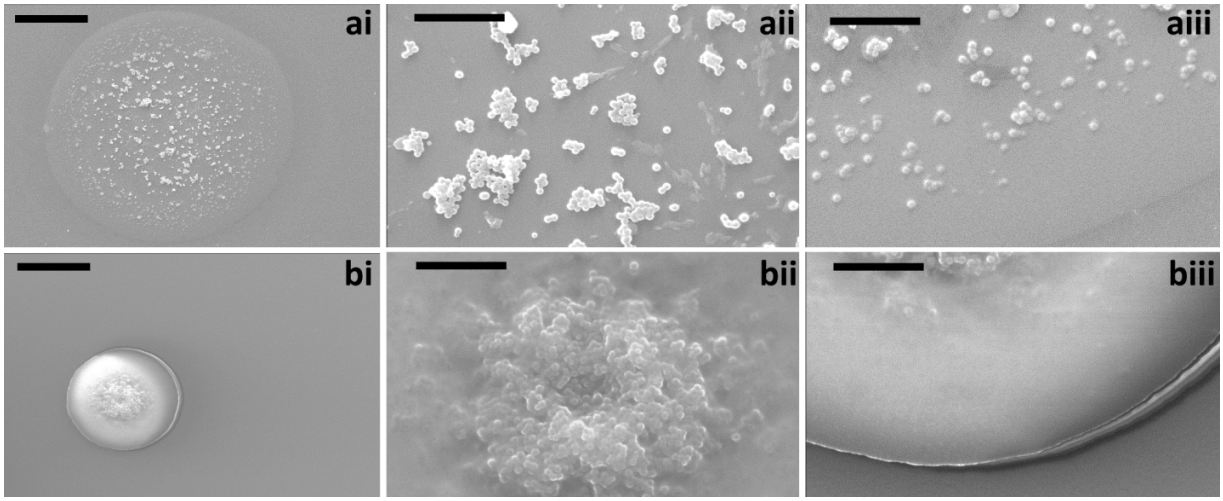

Figure 15. SEM images of deposits from dried 50%v ethanol/water droplets containing 0.1%w 755 nm polystyrene spheres, and a) 0.5%w 300 kg mol^{-1} PSS or b) 3%w 70 kg mol^{-1} PSS. Images show i) the whole deposit, and zooms to ii) the deposit centre, and iii) the contact line. Substrates are glass. Scale bars are 50 μm for the whole deposit and 10 μm for the zooms.

For higher molecular weight samples, the depletion interaction acts over larger distances forming flocs early on in the formation of a central particle group. There is also less mobility of particles within a floc, reducing rearrangement. These flocs do not form many contact points with other flocs in the group so do not create an interconnected structure. The structure can then be pulled outwards/apart by capillary flow (Figure 15a). In contrast, the lower molecular weight samples have a higher number of contact points, such that a single particle may have multiple weak depletion interactions forming a strong interconnected particle floc overall. This large particle floc cannot be separated by capillary flow (Figure 15b).

For a lower molecular weight PSS (35 kg mol^{-1}) at concentrations up to 15%w in water, we observed particle migration to form a collected group of particles, but no aggregation. As the PSS concentration increased, particle motion towards the contact line was reduced in the latter stage of drying, probably due to rapid increase in the viscosity of the solution as the solvent

evaporates. The result was a circular deposit with good radial uniformity and a smaller diameter than the initial droplet (~0.4*R*, see Fig. 11(a))). Increasing the PSS concentration further to 20%w to encourage depletion flocculation resulted in phase separation in the initial solution (50%v ethanol) due to the solubility limit of the PSS. The high polymer content in the 15%w suspension causes a large increase in viscosity throughout drying (particularly near the contact line), which could mean that it is not depletion flocculation that is retaining the central group but a polymer matrix. While the 15%w PSS solution in water does give a dot with a well-defined edge, there is a large amount of polymer deposited on the surface which may be undesirable for applications (a small amount of polymer to act as a binder may be desirable).

Our experiments indicate an optimal polymer molecular weight around 70 kg mol^{-1} for generating a single dense floc of colloidal particles at the centre of the evaporating droplet. Lower molecular weight polymers did not cause obvious depletion flocculation and high concentrations were needed to inhibit radial convection – probably through the rapid increase in viscosity in the latter stages of drying. Higher molecular weight polymers tended to cause flocculation too early and led to a large number of small aggregates that migrated towards the contact line under convective flow. We also found an optimum polymer concentration that induced aggregation at the point where the particles had formed the smallest central disk. Lower polymer concentrations did not prevent radial convection at the end of drying while higher concentrations increased the viscosity and inhibited the inward migration of the particles under Marangoni flow. Polystyrene sphere concentrations of up to 1%v (higher concentrations were not tested), resulted in particle collection and a small central dot deposit (Figure 16).

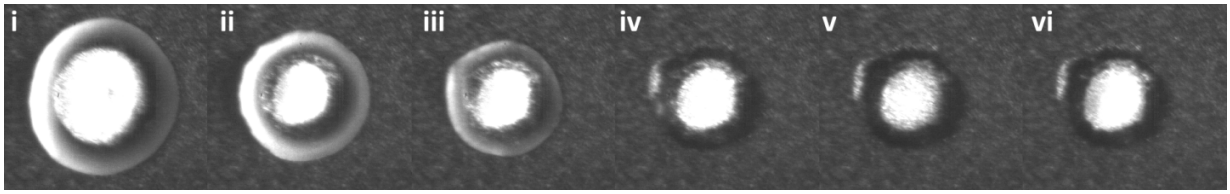

Figure 16. Sequence of images for a drying droplet containing 50%v ethanol/water, 3%w 70 kg mol^{-1} PSS (in water alone) and 1%v 775 nm polystyrene spheres at i) $0.1t_{dry}$, ii) $0.2t_{dry}$, iii) $0.5t_{dry}$, iv) $0.8t_{dry}$, v) $0.9t_{dry}$, vi) $1.0t_{dry}$.

Conclusions

Drying droplets of ethanol/water exhibit Marangoni flows and particle migration, collecting particles in a concentrated central group during the Marangoni flow period. To prevent radial flow subsequently transporting particles to the contact line and forming a ring stain, two strategies were developed to maintain the central group in the deposit. The result was the printing of a small deposit from a large droplet, which may provide a viable mechanism for security printing, where the method must be known to replicate the print consistently. The mechanism described is also a good method for printing high resolution lines for conductive screens.

The first strategy used an evaporation-driven sol-gel transition to prevent particle motion in the gel through elasticity. Once the yield stress of the laponite suspension was sufficient to overcome the capillary flow, particle motion towards the contact line ceased. The recovery time of the network (following break-down in the print-head) needed to be fast enough to form a gel shortly after the Marangoni flow period had ended, but not so fast that migration was inhibited. A lower ethanol concentration and higher laponite concentration proved to produce the best deposits.

The second fixing strategy used polystyrene sulfonate (PSS) to induce depletion flocculation for a range of molecular weights. A higher PSS concentration was required for flocculation when

a lower molecular weight was used, which resulted in more undesirable impurity left in the deposit. For high molecular weights, less PSS was required for flocculation, but the particle flocs formed were loose and not inter-connected. Consequently, capillary flow was able to pull the particle flocs apart and a wide group was formed as a deposit. A molecular weight of 70 kg mol^{-1} gave good interconnectivity between particle flocs at ~ 2%w (in the entire solution), forming a dense, locked structure which was retained at the deposit centre, forming a small dot.

Supporting Information. Additional videos of drying droplets containing laponite or PSS are included corresponding to Figure 1, Figure 8a, Figure 11b/c and Figure 12a. This material is available free of charge via the Internet at http://pubs.acs.org.

ACKNOWLEDGMENT

The authors thank Dr. Olivier Cayre (University of Leeds) for his valued advice, and Dr. P. S. Brown and Prof. J. P. S. Badyal (Durham University) for the coated substrates. This work was supported financially by EPSRC under grant number EP/H018913/1.

REFERENCES

1) R.D. Deegan, O. Bakajin, T.F. Dupont, G. Huber, S.R. Nagel and T.A. Witten, Capillary flow as the cause of ring stains from dried liquid drops, Nature, 1997, 389, 827-829.

2) T.R. Hebner, C.C. Wu, D. Marcy, M.H. Lu and J.C. Sturm, Ink-jet printing of doped polymers for organic light emitting devices, Appl. Phys. Lett., 1998, 72, 5, 519-521.

3) H. Sirringhaus, T. Kawase, R.H. Friend, T. Shimoda, M. Inbasekaran, W. Wu and E.P. Woo, High-resolution inkjet printing of all-polymer transistor circuits, Science, 2000, 290, 5499, 2123-2126.

4) Y. Yang, S-C. Chang, J. Bharathan and J. Liu, Organic/polymeric electroluminescent devices processed by hybrid ink-jet printing, J. Mater. Sci.- Mater. El., 2000, 11, 2, 89-96.

5) D. Soltman and V. Subramanian, Inkjet-printed line morphologies and temperature control of the coffee ring effect, Langmuir, 2008, 24, 5, 2224-2231.

6) S.B. Fuller, E.J. Wilhelm and J.M. Jacobson, Ink-jet printed nanoparticle microelectromechanical systems, J. Microelectromech. Sys., 2002, 11, 1, 54-60.

7) S. Molesa, D.R. Redinger, D.C. Huang and V. Subramanian, High-quality inkjet-printed multilevel interconnects and inductive components on plastic for ultra-low-cost RFID applications, Mat. Res. Soc. Symp. Proc., 2003, 769, 253-258.

8) D. Kim and J. Moon, Highly conductive ink jet printed films of nanosilver particles for printed electronics, Electrochem. Solid St. Lett., 2005, 8, 11, J30-J33.

9) D.J. Lee and J.H. Oh, Shapes and morphologies of inkjet-printed nanosilver dots on glass substrates, Surf. Interface Anal., 2010, 42, 6-7, 1261-1265.

10) T. Okamoto, T. Suzuki and N. Yamamoto, Microarray fabrication with covalent attachment of DNA using Bubble Jet technology, Nature Biotech., 2000, 18, 5, 438-441.

11) E.A. Roth, T. Xu, M. Das, C. Gregory, J.J. Hickman and T. Boland, Inkjet printing for high-throughput cell patterning, Biomater., 2004, 25, 17, 3707-3715.

12) H. Hu and R.G. Larson, Marangoni effect reverses coffee-ring depositions, J. Phys. Chem. B, 2006, 110, 14, 7090-7094.

13) J. Park and J. Moon, Control of colloidal particle deposit patterns within picoliter droplets ejected by ink-jet printing, Langmuir, 2006, 22, 8, 3506-3513.

14) J.A. Lim, W.H. Lee, H.S. Lee, J.H. Lee, Y.D. Park and K. Cho, Self-organization of ink-jet-printed triisopropylsilylethynyl pentacene via evaporation-induced flows in a drying droplet, Adv. Funct. Mater., 2008, 18, 2, 229-234.

15) T. Kajiya, W. Kobayashi, T. Okuzono and M. Doi, Controlling the drying and film formation processes of polymer solution droplets with addition of small amount of surfactants, J. Phys. Chem. B, 2009, 113, 47, 15460-15466.

16) T. Still, P.J. Yunker and A.G. Yodh, Surfactant-induced Marangoni eddies alter the coffee-rings of evaporating colloidal drops, Langmuir, 2012, 28, 11, 4984-4988.

17) H. Hu and R.G. Larson, Analysis of the effects of Marangoni stresses on the microflow in an evaporating sessile droplet, Langmuir, 2005, 21, 9, 3963-3971.

18) Y. Hamamoto, J.R.E. Christy and K. Sefiane, The flow characteristics of an evaporating ethanol water mixture droplet on a glass substrate, J. Therm. Sci. Technol., 2012, 7, 3, 425-436.

19) E.L. Talbot and A. Berson and C.D. Bain, Drying and deposition of picolitre droplets of colloidal suspensions in binary solvent mixtures, NIP28: 28th International Conference on Digital Printing Technologies, and Digital Fabrication 2012, September 2012, The Society for Imaging Science and Technology, 2012, 2, 420-423, ISSN 978-0-89208-301-5.

20) E.L. Talbot, A. Berson and C.D. Bain, Internal flows and particle transport inside picoliter droplets of binary solvent mixtures, NIP29: 29th International Conference on Digital Printing

Technologies, and Digital Fabrication 2013, September/October 2013, The Society for Imaging Science and Technology, 2013, 28, 307-312, ISSN 978-0-89208-307-7.

21) E.L. Talbot, L. Yang, A. Berson and C.D. Bain, Control of particle distribution in inkjet printing through an evaporation-driven sol-gel transition, Appl. Mater. Interf., 2014, 6, 12, 9572-9583.

22) A. Mourchid, A. Delville and P. Levitz, Sol-gel transition of colloidal suspensions of anisotropic particles of laponite, Faraday Diskuss., 1995, 101, 275-285.

23) J.E. Seebergh and J.C. Berg, Depletion flocculation of aqueous, electrosterically-stabilized latex dispersions, Langmuir, 1994, 10, 2, 454-463.

24) A. Sharma, S.N. Tan and Y. Walz, Effect of nonadsorbing polyelectrolytes on colloidal interactions in aqueous mixtures, J. Colloid Interf. Sci., 1997, 191, 1, 236-246.

25) A. Sharma, S.N. Tan and Y. Walz, Measurement of colloidal stability in solutions of simple, nonadsorbing polyelectrolytes, J. Colloid Interf. Sci., 1997, 190, 2, 392-407.

26) J.L. Burns, Y. Yan, G.J. Jameson and S. Biggs, The effect of molecular weight of nonadsorbing polymer on the structure of depletion-induced flocs, J. Colloid Interf. Sci., 2002, 247, 24-32.

27) I. Woodward, W.C.E. Schofield, V. Roucoules and J.P.S. Badyal, Super-hydrophobic Surfaces Produced by Plasma Fluorination of Polybutadiene Films, Langmuir, 2003, 19, 3432-3438.

28) N.N. Herrera, J.-M. Letoffe and J.-L. Putaux, Aqueous dispersions of silane-functionalized laponite clay platelets: A first step toward the elaboration of water-based polymer/clay nanocomposites, Langmuir, 2004, 20, 5, 1564-1571.

29) H. N. Yow and S. Biggs, Probing the stability of sterically stabilized polystyrene particles by centrifugal sedimentation, Soft Matter, 2013, 9, 10031-10041.